

# Thermal Memory Effect in Polymer Optical Fibers

Kazunari Minakawa, Neisei Hayashi, Yosuke Mizuno, *Member, IEEE*, and Kentaro Nakamura, *Member, IEEE*

**Abstract**—The basic properties of a thermal memory effect of polymer optical fibers (POFs) are experimentally investigated. We measure the thermally induced loss as a function of time at several high temperatures, and find that the loss becomes almost constant after heating for  $\sim 200$  s. The loss remains unchanged even after the heated section is cooled to room temperature. We subsequently measure the optical time-domain reflectometry traces under three different conditions: 1) before a POF section is heated; 2) shortly after the POF section is heated at high temperature; and 3) after the heated section is cooled to room temperature. The traces measured under 2) and 3) are moderately identical, which indicates that the thermal memory effect can be exploited in developing excess-heat detecting system in future.

**Index Terms**—Polymer optical fibers, temperature sensing, optical time-domain reflectometry, thermal memory effect.

## I. INTRODUCTION

FIBER-OPTIC strain and temperature sensors have been extensively studied as promising tools for structural health monitoring [1]–[10]. Conventionally, their sensing heads were mainly composed of glass optical fibers, which cannot withstand strain of over several percent. To tackle this problem, strain and temperature sensors using polymer optical fibers (POFs) [11] have attracted a lot of attention, because POFs are so flexible that they can withstand larger strain of several tens of percent (even 100% [12]). To date, various strain and temperature sensors using POFs have been developed, including those based on fiber Bragg gratings [13], [14], modal interference [15]–[17], Brillouin scattering [18]–[25], and Rayleigh scattering [26]–[29].

One of the unique features of POF-based strain sensors is what we call a “strain memory effect” [12], [19], [20], [26], [27], with which POFs themselves store the information (magnitude and location) of applied large strain even after the strain is released. This nature is caused by plastic deformation of the polymer materials. We expect that, by exploiting this effect, we need not always put expensive analyzers at the ends of the sensing fibers; after earthquakes etc, an officer has

only to go round with a single analyzer. Then, the application range of fiber-optic sensing technology, which has been limited only to large-scale civil structures owing to its high cost, can be extended to smaller-scale multi-family residences and individual houses.

In the meantime, the optical loss of POFs is dependent on temperature. The loss is reported to increase with increasing temperature [25], [26], and especially at high temperature of  $> 100$  °C, irreversible loss has been observed [25], [26]. In addition, we have recently found that, when a POF sample is heated at such high temperature and then cooled to room temperature, its Brillouin frequency shift (BFS) does not return to the initial value at room temperature [22]. These results suggest the existence of a useful “thermal memory effect” of POFs, on the detail of which no report has been provided yet. This effect might be exploited to detect the excess heat only by interrogating the POFs later, for instance, at regular (periodic) inspections.

In this work, we experimentally investigate the “thermal memory effect” of POFs. First, thermally induced loss is plotted as a function of time at several high temperatures. The loss becomes almost constant after heating of the POFs for  $\sim 200$  s. We then measured the optical time-domain reflectometry (OTDR) traces under three different conditions: (1) before a POF section is heated, (2) after the POF section is heated at high temperature for a sufficiently long time, and (3) after the heated section is cooled to room temperature. By comparing these results, we discuss the future prospects of the thermal memory effect.

## II. MEASUREMENT APPARATUS

As POFs to be measured, we used perfluorinated graded-index (PFGI-) POFs [30] with three-layered structure (Ginover; Sekisui Chemical Co., Japan): core (50  $\mu\text{m}$  diameter), cladding (100  $\mu\text{m}$  diameter), and overcladding (750  $\mu\text{m}$  diameter). The core and cladding layers are composed of doped and undoped polyperfluorobutenylvinyl ether, respectively. The refractive index at the center of the core is 1.356, while that of the cladding is 1.342. The protecting overcladding layer consists of polycarbonate. The propagation loss is relatively low in a wide wavelength range from  $\sim 600$  nm to 1500 nm [30].

One of the most popular distributed loss sensing techniques is OTDR based on Rayleigh scattering [31], [32]. In general, short optical pulses ( $\sim 10$  ns) are launched into a fiber under test (FUT), and the Rayleigh-backscattered signal is detected on the same end. The events that increase the optical loss (bending, connection, etc) are spatially resolved with a time-of-flight technique, i.e., using a famous equation:  $L = c \Delta t / 2n$ ,

Manuscript received February 19, 2015; revised March 25, 2015; accepted April 6, 2015. Date of publication April 10, 2015; date of current version June 9, 2015. This work was supported in part by the Grants-in-Aid for Young Scientists (A) under Grant 25709032, in part for the Challenging Exploratory Research under Grant 26630180 through the Japan Society for the Promotion of Science (JSPS), and in part by the Research Grants through the General Sekiyu Foundation, Iwatani Naoji Foundation, and SCAT Foundation. The work of N. Hayashi was supported by the Grant-in-Aid for JSPS Fellows under Grant 25007652.

The authors are with the Precision and Intelligence Laboratory, Tokyo Institute of Technology, Yokohama 226-8503, Japan (e-mail: kminakawa@sonic.pi.titech.ac.jp; hayashi@sonic.pi.titech.ac.jp; ymizuno@sonic.pi.titech.ac.jp; knakamura@sonic.pi.titech.ac.jp).

Color versions of one or more of the figures in this letter are available online at <http://ieeexplore.ieee.org>.

Digital Object Identifier 10.1109/LPT.2015.2421950

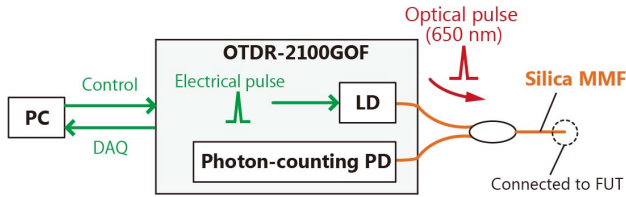


Fig. 1. Schematic of OTDR-2100GOF system. DAQ, data acquisition; LD, laser diode; MMF, multimode fiber; PC, personal computer; PD, photo detector.

where  $L$  is the relative position along the FUT,  $c$  is the light velocity in vacuum,  $\Delta t$  is the time delay between pulse injection and detection, and  $n$  is the refractive index of the FUT core.

In order to detect the weak backscattered light in PFGI-POFs with high sensitivity, a commercial photon-counting OTDR system (OTDR-2100GOF; Scientex Inc., Japan) was employed in this experiment. The schematic of the OTDR system is depicted in Fig. 1. A semiconductor laser diode (LD) outputs an optical pulse at 650 nm with a peak power of several tens of milliwatts, the width of which can be set to either 2 or 10 ns by direct modulation of the driving current (via a personal computer (PC)). The optical pulse is directed to the FUT via a silica-based multimode fiber (MMF) coupler. The backscattered light is then input to a photon-counting photo detector (PD), with which the optical intensity is detected as pulse density of photons, generating a density-modulated pulse train. By repeatedly recording many results for the same inputs, a histogram plotted as a function of the location along the FUT is obtained, which corresponds to the conventional OTDR trace (a figure intelligibly explaining this mechanism is found in Ref [26]). Note that, according to the manufacturer, the vertical axis of the OTDR trace measured using this system is not the backscattered power itself but an attenuation rate to an internally defined reference value (not described in the manual).

### III. EXPERIMENTS

First, we clarify the heating duration required for the thermally induced loss in POFs to be constant. Subsequently, we verify and discuss the thermal memory effect of POFs by comparing the measured OTDR traces.

#### A. Temporal Dependence of Thermally Induced Loss

The experimental setup for measuring the temporal dependence of the thermally induced loss in POFs is shown in Fig. 2. The continuous wave (CW) output from an LD at 641 nm with a power of  $\sim 1$  mW was directly coupled to a PFGI-POF and injected into a silica GI-MMF via butt-coupling using an “SC” adaptor [18], and the transmitted power was monitored using an optical power meter (PM). A 150-mm-long section of the POF was guided in a furnace placed on a heater; the ambient temperature of the POF in the furnace was precisely controlled using a thermocouple.

The measured temporal variations of the thermally induced loss at 115, 120, 125, 129, and 133 °C are shown in Fig. 3(a).

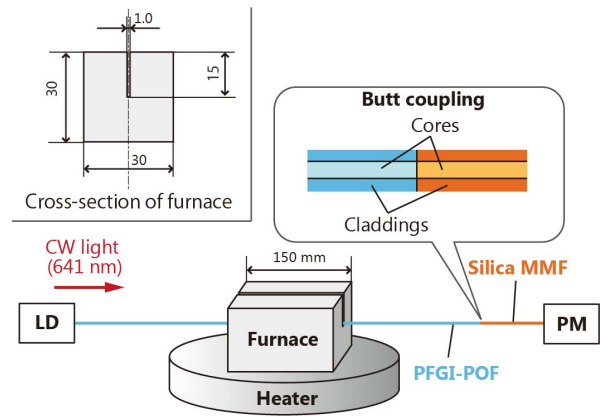


Fig. 2. Experimental setup for measuring temporal variations of the loss thermally induced in the PFGI-POF. The top-left inset shows the cross-sectional view of the furnace; all the values are in the unit of millimeters.

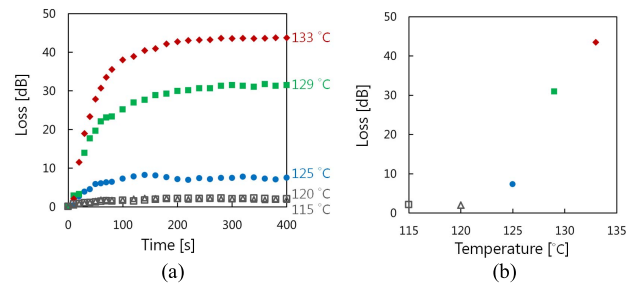


Fig. 3. (a) Temporal variations of the loss thermally induced in the PFGI-POF. (b) Thermally induced loss measured at  $t = 400$  s, plotted as a function of heating temperature.

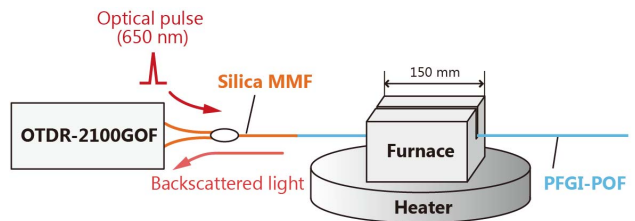


Fig. 4. Experimental setup for evaluating the thermal memory effect in PFGI-POFs using OTDR.

At 115 and 120 °C, the loss was within the range of measurement error ( $\pm 2$  dB; caused by the fluctuations of the LD output and by the slight tension applied to the heated section), while at 125, 129, and 133 °C, the loss clearly increased with time  $t$ . Here,  $t = 0$  is defined as the moment at which the POF section was vertically introduced into the furnace using motorized stages. When the heated section was above  $\sim 120$  °C, we could observe the strong scattering of the incident light to the FUT along the section. This result indicates that the thermally induced loss was generated as the radiation loss along the heated section. The induced loss increased during  $t \approx 100$ – $200$  s, and then became almost constant.

Figure 3(b) shows the heating temperature dependence of the induced loss measured at  $t = 400$  s. The loss was negligible below  $\sim 120$  °C, but above  $\sim 120$  °C, it became higher with increasing temperature. The amount of this loss

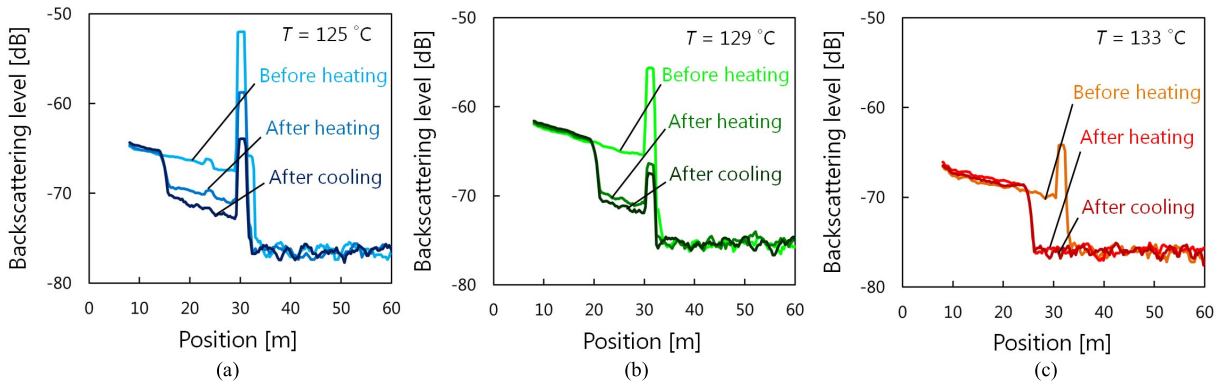


Fig. 5. Measured OTDR traces before heating, after heating (at (a) 125 °C, (b) 129 °C, and (c) 133 °C), and after cooling.

remained almost identical even after the heated POF section was cooled to room temperature. This threshold temperature is higher than the glass transition temperature of the core/cladding material by  $\sim 15$  °C. Considering that the phase transition of polymer materials to rubbery state generally occurs in the range  $\sim 10$ – $20$  °C around the glass transition temperature [33] and that the core temperature should be lower than the ambient temperature measured using a thermocouple, it is strongly implied that the thermal induction of the loss in POFs originates from the fluctuation of the interfacial surface between the core and cladding which was induced by the phase transition of the core and cladding to rubbery state.

### B. Evaluation of Thermal Memory Effect

We evaluate the thermal memory effect in POFs in distributed sensing using the experimental setup shown in Fig. 4. The OTDR system was connected to a PFGI-POF with a length of roughly 30 m, and its 150-mm-long section was heated in the furnace, the temperature of which was controlled in the same manner as in Section III. A. The optical pulse width was set to 2 ns, corresponding to  $\sim 220$ -mm spatial resolution in the POF. When the POF section was heated, high temperature environment was maintained for at least 600 s (sufficiently longer than 200 s; see Fig. 3(a)) to ensure that the thermally induced loss grew constant.

Figs. 5(a)–(c) show the measured OTDR traces under three conditions: (1) at room temperature, before heating the POF section; (2) shortly after heating the section for a sufficiently long time at high temperatures (125, 129, and 133 °C in Figs. 5 (a), (b), and (c), respectively); and (3) at room temperature, after cooling the heated section. The reflected signal was integrated for 600,000 optical pulses. The data at positions of  $< 8$  m were not presented due to the signal fluctuations inevitably caused by the system. The signal levels at the position of 8 m were not the same for the three cases because of the unstable butt-coupling of the PFGI-POF and the silica GI-MMF [18].

In the case of 125 °C (Fig. 5(a)), the POF length was 29 m; at the open end of the POF, Fresnel reflection signal was observed. Before heating the POF section, no drastic drop was observed in the OTDR trace. After the POF section was heated, a drastic drop of  $\sim 3.5$  dB was observed at the

position of  $\sim 15$  m, where the heated section was located. Here, the amount of the drop (3.5 dB) did not agree with the loss observed in Fig. 3(b), which seems to be caused by the specification of the OTDR system (see Section II) and by the difference of the LD outputs, i.e., CW or pulses. After cooling the heated section, the drop became slightly larger ( $\sim 4.4$  dB) probably because the POF was damaged when it was vertically taken out of the furnace using the stages. Even if so, this result proves that, though detailed quantitative evaluation is difficult at present, the OTDR trace when the POF was locally heated at high temperature in the past can be obtained at a later time, i.e., the operation of the thermal memory effect of the POF. It is also notable that no quantifiable reflection was induced at the heated section, which might be a cost-effective method (with no need for additional devices) for suppressing the Fresnel reflection to improve the signal-to-noise ratio in POF-based Brillouin optical correlation-domain reflectometry [10], [34] (a drastic increase in loss simply by bending is difficult for POFs with large cores [30]).

In the case of 129 °C (Fig. 5(b)), the POF length was  $\sim 30$  m. Similar behaviors were observed; the drop of the OTDR trace at the heated section (position =  $\sim 20$  m) was  $\sim 5.5$  dB after heating and  $\sim 6.0$  dB after cooling, which were higher than those at 125 °C, as is expected in Fig. 3(b). In the case of 133 °C (Fig. 5(c)), the POF length was  $\sim 31$  m. Basically, similar behaviors were observed, but the drop at the heated section (position =  $\sim 25$  m) was so large ( $\gg 8.0$  dB) that the trace was buried by the noise floor.

Thus, the thermal memory effect in POFs was confirmed, but the temperature range at which this effect can be exploited is limited to  $\sim 120$ – $129$  °C in this experiment. Such temperature range could be set somewhat arbitrarily in future, because the glass transition temperature in polymer materials, which probably affects this effect, can be controlled by adding plasticizers and/or by copolymerizing different materials [35]. This will be a useful feature in designing practical excess-heat detectors based on this thermal effect of POFs.

## IV. CONCLUSION

The fundamental properties of the “thermal memory effect”—an attractive function of POF-based temperature sensors—was experimentally investigated. First, we measured

the loss thermally induced at several high temperatures as a function of time. When the temperature was higher than  $\sim 120$  °C, the loss grew almost constant after heating the POFs for  $\sim 200$  s. This loss was maintained even after the POFs were cooled to room temperature. Next, we measured the OTDR traces under three different conditions: (1) before a POF section was heated, (2) after the POF section was heated at high temperature for a time much longer than 200 s, and (3) after the heated section was cooled to room temperature. The traces obtained under (2) and (3) did not exhibit large change irrespective of the heating temperature, which indicated that the thermal memory effect will be useful in developing excess-heat detecting systems in the near future. What remain to be solved include the improvement of quantitative evaluation of temperature, the broadening of the temperature range in which this effect can be exploited, and the discrimination of strain and thermal memory effects.

#### ACKNOWLEDGMENT

The authors are indebted to Scientex Inc., Japan, and Hiroki Tanaka, Tokyo Institute of Technology, Japan, for their experimental assistance. They also acknowledge the staff of the Technical Department, Tokyo Institute of Technology, Japan, for fabricating the furnace used in the experiments.

#### REFERENCES

- [1] K. O. Hill, Y. Fujii, D. C. Johnson, and B. S. Kawasaki, "Photosensitivity in optical fiber waveguides: Application to reflection filter fabrication," *Appl. Phys. Lett.*, vol. 32, no. 10, pp. 647–649, 1978.
- [2] P. C. Won, J. Leng, Y. Lai, and J. A. R. Williams, "Distributed temperature sensing using a chirped fibre Bragg grating," *Meas. Sci. Technol.*, vol. 15, no. 8, pp. 1501–1505, 2004.
- [3] K. Hotate and K. Kajiwara, "Proposal and experimental verification of Bragg wavelength distribution measurement within a long-length FBG by synthesis of optical coherence function," *Opt. Exp.*, vol. 16, no. 11, pp. 7881–7887, 2008.
- [4] M. A. Farahani and T. Gogolla, "Spontaneous Raman scattering in optical fibers with modulated probe light for distributed temperature Raman remote sensing," *J. Lightw. Technol.*, vol. 17, no. 8, pp. 1379–1391, Aug. 1999.
- [5] J. P. Dakin, D. J. Pratt, G. W. Bibby, and J. N. Ross, "Distributed optical fibre Raman temperature sensor using a semiconductor light source and detector," *Electron. Lett.*, vol. 21, no. 13, pp. 569–570, 1985.
- [6] T. Horiguchi, T. Kurashima, and M. Tateda, "Tensile strain dependence of Brillouin frequency shift in silica optical fibers," *J. Lightw. Technol.*, vol. 1, no. 5, pp. 107–108, May 1989.
- [7] D. Garus, K. Krebber, F. Schliep, and T. Gogolla, "Distributed sensing technique based on Brillouin optical-fiber frequency-domain analysis," *Opt. Lett.*, vol. 21, no. 17, pp. 1402–1404, 1996.
- [8] K. Hotate and T. Hasegawa, "Measurement of Brillouin gain spectrum distribution along an optical fiber using a correlation-based technique—Proposal, experiment and simulation—," *IEICE Trans. Electron.*, vol. E83-C, no. 3, pp. 405–412, Mar. 2000.
- [9] T. Kurashima, T. Horiguchi, H. Izumita, S. Furukawa, and Y. Koyamada, "Brillouin optical-fiber time domain reflectometry," *IEICE Trans. Commun.*, vol. E76-B, no. 4, pp. 382–390, Apr. 1993.
- [10] Y. Mizuno, W. Zou, Z. He, and K. Hotate, "Proposal of Brillouin optical correlation-domain reflectometry (BOCDR)," *Opt. Exp.*, vol. 16, no. 16, pp. 12148–12153, 2008.
- [11] M. G. Kuzyk, *Polymer Fiber Optics: Materials, Physics, and Applications*. Boca Raton, FL, USA: CRC Press, 2006.
- [12] H. Ujihara, N. Hayashi, M. Tabaru, Y. Mizuno, and K. Nakamura, "Measurement of large-strain dependence of optical propagation loss in perfluorinated polymer fibers for use in seismic diagnosis," *IEICE Electron. Exp.*, vol. 11, no. 17, p. 20140707, 2014.
- [13] Z. Xiong, G. D. Peng, B. Wu, and P. L. Chu, "Highly tunable Bragg gratings in single-mode polymer optical fibers," *IEEE Photon. Technol. Lett.*, vol. 11, no. 3, pp. 352–354, Mar. 1999.
- [14] H. Dobb, D. J. Webb, K. Kalli, A. Argyros, M. C. Large, and M. A. van Eijkelenborg, "Continuous wave ultraviolet light-induced fiber Bragg gratings in few- and single-mode microstructured polymer optical fibers," *Opt. Lett.*, vol. 30, no. 24, pp. 3296–3298, 2005.
- [15] J. Huang *et al.*, "Polymer optical fiber for large strain measurement based on multimode interference," *Opt. Lett.*, vol. 37, no. 20, pp. 4308–4310, 2012.
- [16] G. Numata, N. Hayashi, M. Tabaru, Y. Mizuno, and K. Nakamura, "Ultra-sensitive strain and temperature sensing based on modal interference in perfluorinated polymer optical fibers," *IEEE Photon. J.*, vol. 6, no. 5, Oct. 2014, Art. ID 6802306.
- [17] G. Numata, N. Hayashi, M. Tabaru, Y. Mizuno, and K. Nakamura, "Strain and temperature sensing based on multimode interference in partially chlorinated polymer optical fibers," *IEICE Electron. Exp.*, vol. 12, no. 2, p. 20141173, 2015.
- [18] Y. Mizuno and K. Nakamura, "Experimental study of Brillouin scattering in perfluorinated polymer optical fiber at telecommunication wavelength," *Appl. Phys. Lett.*, vol. 97, no. 2, p. 021103, 2010.
- [19] N. Hayashi, Y. Mizuno, and K. Nakamura, "Brillouin gain spectrum dependence on large strain in perfluorinated graded-index polymer optical fiber," *Opt. Exp.*, vol. 20, no. 19, pp. 21101–21106, 2012.
- [20] N. Hayashi, K. Minakawa, Y. Mizuno, and K. Nakamura, "Brillouin frequency shift hopping in polymer optical fiber," *Appl. Phys. Lett.*, vol. 105, no. 9, p. 091113, 2014.
- [21] N. Hayashi, Y. Mizuno, and K. Nakamura, "Distributed Brillouin sensing with centimeter-order spatial resolution in polymer optical fibers," *J. Lightw. Technol.*, vol. 32, no. 21, pp. 3999–4003, Nov. 1, 2014.
- [22] N. Hayashi, H. Fukuda, Y. Mizuno, and K. Nakamura, "Observation of Brillouin gain spectrum in tapered polymer optical fiber," *J. Appl. Phys.*, vol. 115, no. 17, p. 173108, 2014.
- [23] A. Minardo, R. Bernini, and L. Zeni, "Distributed temperature sensing in polymer optical fiber by BOFDA," *IEEE Photon. Technol. Lett.*, vol. 26, no. 4, pp. 387–390, Feb. 15, 2014.
- [24] Y. Dong, P. Xu, H. Zhang, Z. Lu, L. Chen, and X. Bao, "Characterization of evolution of mode coupling in a graded-index polymer optical fiber by using Brillouin optical time-domain analysis," *Opt. Exp.*, vol. 22, no. 22, pp. 26510–26516, 2014.
- [25] K. Minakawa *et al.*, "Wide-range temperature dependences of Brillouin scattering properties in polymer optical fiber," *Jpn. J. Appl. Phys.*, vol. 53, no. 4, p. 042502, 2014.
- [26] I. R. Husdi, K. Nakamura, and S. Ueha, "Sensing characteristics of plastic optical fibres measured by optical time-domain reflectometry," *Meas. Sci. Technol.*, vol. 15, no. 8, pp. 1553–1559, 2004.
- [27] K. Nakamura, I. R. Husdi, and S. Ueha, "A distributed strain sensor with the memory effect based on the POF OTDR," *Proc. SPIE*, vol. 5855, pp. 807–810, Aug. 2005.
- [28] S. Liehr, N. Nother, and K. Krebber, "Incoherent optical frequency domain reflectometry and distributed strain detection in polymer optical fibers," *Meas. Sci. Technol.*, vol. 21, no. 1, p. 017001, 2010.
- [29] C. Saunders and P. J. Scully, "Sensing applications for POF and hybrid fibres using a photon counting OTDR," *Meas. Sci. Technol.*, vol. 18, no. 3, pp. 615–622, 2007.
- [30] Y. Koike and M. Asai, "The future of plastic optical fiber," *NPG Asia Mater.*, vol. 1, no. 1, pp. 22–28, 2009.
- [31] M. K. Barnoski, M. D. Rourke, S. M. Jensen, and R. T. Melville, "Optical time domain reflectometer," *Appl. Opt.*, vol. 16, no. 9, pp. 2375–2379, 1977.
- [32] Y. Koyamada, M. Imahama, K. Kubota, and K. Hogari, "Fiber-optic distributed strain and temperature sensing with very high measurement resolution over long range using coherent OTDR," *J. Lightw. Technol.*, vol. 27, no. 9, pp. 1142–1146, May 1, 2009.
- [33] M. Chanda and S. K. Roy, *Plastics Technology Handbook*, 3rd ed. Boca Raton, FL, USA: CRC Press, 1998.
- [34] N. Hayashi, Y. Mizuno, and K. Nakamura, "Suppression of ghost correlation peak in Brillouin optical correlation-domain reflectometry," *Appl. Phys. Exp.*, vol. 7, no. 11, p. 112501, 2014.
- [35] K. Koike, H. Teng, Y. Koike, and Y. Okamoto, "Effect of dopant structure on refractive index and glass transition temperature of polymeric fiber-optic materials," *Polym. Adv. Technol.*, vol. 25, no. 2, pp. 204–210, 2014.